Hindawi
Journal of Sensors
Volume 2022, Article ID 4782855, 9 pages
https://doi.org/10.1155/2022/4782855

Research Article

Influence of Imperfect Faraday Rotation Mirror on All-Fiber Optic Current Sensor

Jianhua Wu,[1,2] **Xiaofeng Zhang**,[1] **and Liang Chen**[1]

[1]*College of Electrical Engineering, Naval University of Engineering, Wuhan 4300331, China*
[2]*Unit No. 92853, Huludao 125106, China*

Correspondence should be addressed to Liang Chen; 15038513@alu.hdu.edu.cn

Received 5 May 2022; Revised 24 May 2022; Accepted 27 May 2022; Published 7 June 2022

Academic Editor: Carlos Marques

The effects of the Faraday rotation mirror on the all-fiber optic current sensor (AFOCS) are studied in this paper. The reflectivity degradation of FRM with the long-term operation, the misalignment of the optical axis between FRM and the sensing fiber, and the influence of temperature fluctuation on FRM are modeled and simulated in this paper. The effect of temperature is the biggest obstacle to the application of the Faraday rotation mirror, while other factors can be easy to overcome by the data processing method. The experiments are designed and realized for verification. The temperature fluctuation range is related to the measured electric current to satisfy the required accuracy for IEC 60044-8 class 0.2S.

1. Introduction

With many unique advantages compared to traditional sensors, optical fiber sensors have been studied and applied to many different areas [1–5]. As a potential substitute for the traditional electromagnetic current transformer in power industry, the all-fiber optic current sensor (AFOCS) has many advantages, e.g., immunity against electromagnetic interference, high sensitivity, wide dynamic range, measuring AC and DC simultaneous, light weight, and small size [6, 7]. Due to these intrinsic advantages, AFOCS has been widely used in many electric current measurement fields, such as the electrolytic aluminium industry [8], high voltage direct current transmission system [9], international thermonuclear experimental reactor [10], and ship leakage current measurement [11].

Accuracy is one of the most important factors restricting the rapid development of AFOCS. Therefore, improving the accuracy has attracted the attention of many researchers. The first factor that affects the accuracy is the imperfect device. The defective manufacture of the polarizer [12] and polarization-dependent crosstalk [13] will affect the extinction ratio and lead to the relative error. The second factor is the principal axes angle offsets, which are the essential factors affecting the output errors of AFOCS [14, 15]. The last factor is the external interference, such as the temperature and vibration, which will affect the relative error and scale factor [16, 17]. However, there is little literature on the reflection unit [18].

The influence of the Faraday rotation mirror (FRM) on AFOCS focuses on two aspects. One is the reflected light energy, which affects the light intensity detected by the photodetector, while the light intensity affects the signal-to-noise ratio [19]. The other is to adjust the polarization state of reflected light, eliminate the influence of reciprocal linear birefringence, and improve the system accuracy [20]. However, due to the limitation of the manufacturing process level, FRM is usually imperfect [21]. At the same time, FRM is sensitive to temperature [22], and the polarization characteristics of silver thin film mirror typically change with the ambient temperature [23]. Therefore, the features of FRM must be affected by the temperature. In this paper, the influence of FRM on relative error is investigated by modelling and simulation. Experiments were designed and

realized to verify the theoretical analysis and measure the temperature coefficient of FRM. Finally, the comprehensive influence of FRM on AFOCS is obtained.

The remainder of the paper is organized as follows. Section 2 is about the operation principle. The optical design and the data processing method are briefly introduced in this part. Section 3 is the modelling and simulation. We modeled and simulated the influence of FRM on the system accuracy by reflectivity, the misalignment of the optical axis, and the temperature. The experiment and discussion are in Section 4. The last section is the conclusion.

2. The Operating Principle

As the most mature structure of AFOCS, the reflective interferometer current sensor is mainly composed of a light source, an optical system, and a data processing unit [6]. As the key of the optical system, the sensing head usually includes a quarter-wave plate, a sensing fiber ring, and a reflection unit. A phase modulator is introduced to improve the anti-interference ability of the system with phase modulation technology [24]. The structure of AFOCS is shown in Figure 1.

The dotted black line denotes a single-mode fiber for energy transmission. The dot-and-dash line represents the polarization-maintaining fiber used to maintain the polarization state of the light. The solid black line expresses the sensing fiber, which is spun highly birefringent fiber. The arrow indicates the direction of electronic signal transmission. The working principle of the system is based on the Faraday effect and Ampere Circuital Theorem, which is described in Reference 24. When the mirror is the FRM, the detected intensity resulting from the interference is given by

$$I_{\text{out}} = kP_0 \frac{1 + \cos\left(\theta_{\text{F}}\text{-}\Delta\varphi\right)}{2}, \tag{1}$$

where k denotes the scale factor related to optical path loss and photoelectric conversion rate of photodetector, P_0 represents the superluminescent diode optical power, and $\Delta\varphi$ denotes the phase difference modulated by the phase modulator. $\theta_{\text{F}} = 4NVI + \pi$ is the state of the polarization (SOP) rotation angle, where Nexpresses the number of turns of the sensing fiber wrapped around the current-carrying wire, I denotes the electric current in the current-carrying wire, and V represents the Verdet constant of the sensing fiber. The Verdet constant is affected by the operating wavelength, material properties, and temperature [25].

The first harmonic method [24] is used for data demodulation, and the Faraday rotation angle is

$$\theta_F = \arcsin\left(-\frac{U_1}{J_1(\delta)\cdot kP_0}\right) \approx -\frac{U_1}{J_1(\delta)\cdot kP_0}, \tag{2}$$

where $U_1 = -P_0 \cdot \sin\theta_F \cdot J_1(\delta)$ denotes the result of correlation demodulation, $J_1(\delta)$ represents the first-order Bessel function of the first kind, δ is the modulation amplitude, which is usually 1.84 V to get the maximum of $J_1(\delta)$, and k and P_0 are the same as Equation (1).

3. Modeling and Simulation

The relative error is used to describe the effect of FRM on the AFOCS. The relative error η is given by

$$\eta = \left|\frac{\Delta\theta_F}{\theta_F}\right| \times 100\%, \tag{3}$$

where $\Delta\theta_F$ denotes the difference of the Faraday rotation angle due to the change of the reflection unit and θ_F denotes the Faraday rotation angle when the reflection unit is perfect. This paper is mainly about the effect of FRM on AFOCS, so it is assumed that the other parts of the optical system are excellent.

3.1. Effect of Reflectivity. The reflectivity of FRM will decline after a long-term online operation. The rotation angle of SOP to be measured will drift with the reflectivity of FRM. The drift of SOP rotation angle is

$$\Delta\theta_F = \frac{k_2 U_1}{J_1(\delta)\cdot kP_0} - \frac{U_1}{J_1(\delta)\cdot kP_0}, \tag{4}$$

where k_2 denotes the reflectivity of FRM after a long-time online operation, $k_2 < 1$.

Substituting Equations (2) and (4) into Equation (3), the relative error is given by

$$\eta = |k_2 - 1| \times 100\%, \tag{5}$$

where η and k_2 are the same as Equations (3) and (4).

The reflectivity of FRM is 100% and 99% in the perfect and actual conditions, respectively. The relationship between the relative error and the reflectivity is shown in Figure 2.

The relative error will increase as the reflectivity of FRM declines, as shown in Figure 2. When the reflectivity drift is over 0.2%, AFOCS cannot satisfy the required accuracy for IEC 60044-8 class 0.2S [26].

Harmonic division demodulation method could be applied to eliminate the effect of the energy fluctuation on the relative error [27]. The SOP rotation angle is

$$\theta_F = \arctan\left(-\frac{J_2(\delta)\cdot U_1}{J_1(\delta)\cdot U_2}\right), \tag{6}$$

where $U_2 = P_0 \cdot \cos\theta_F \cdot J_2(\delta)$ and $J_2(\delta)$ denotes the second-order Bessel functions of the first kind. The SOP rotation angle has nothing to do with the light intensity, according to Equation (6). The influence of reflectivity is eliminated using this demodulation method.

3.2. Effect of the Misalignment of Optical Axis. FRM consists of a nonreciprocal 45 deg rotator (45 deg Faraday rotator) followed by a coated mirror [20, 21], as shown in Figure 3.

There is a fusion point between FRM and the sensing fiber, as shown in Figure 3. A polarization-maintaining fiber

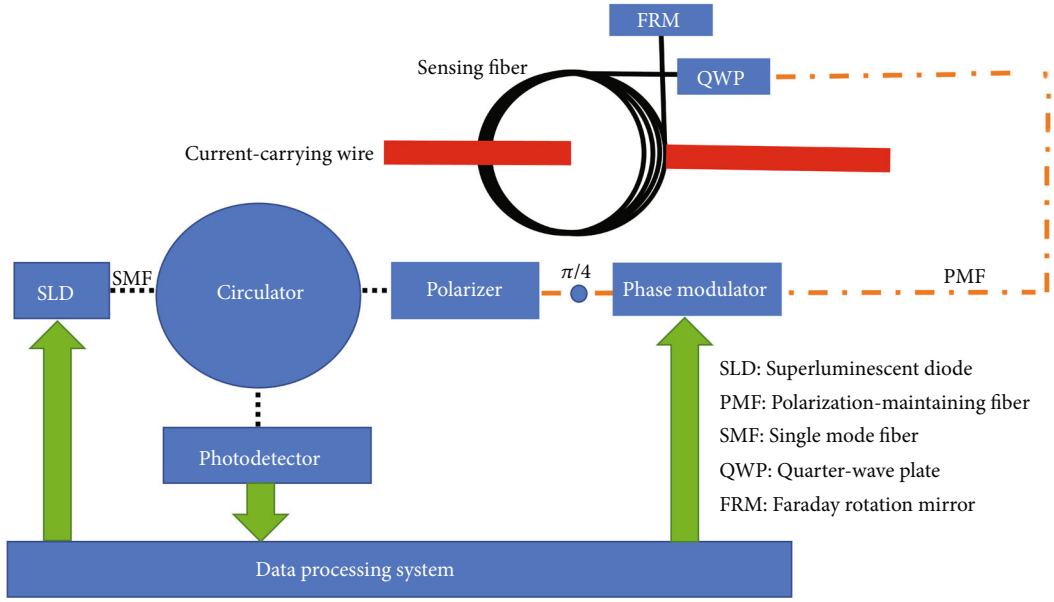

Figure 1: Reflective interferometer current sensor.

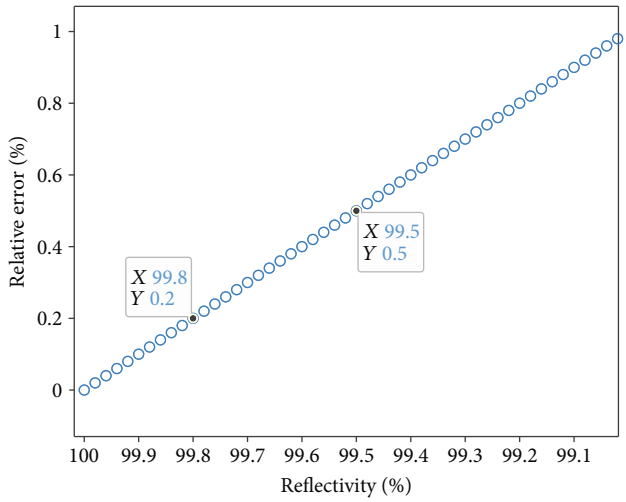

Figure 2: Relationship between the relative error and reflectivity.

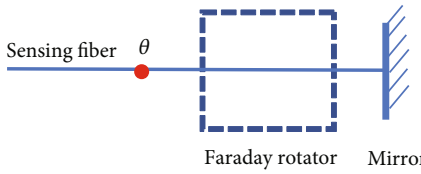

Figure 3: Faraday rotation mirror.

fusion splicer carries out the optical axis to axis fusion. The cross-section of alignment is shown in Figure 4.

The x-axis and y-axis in solid lines represent the sensing fiber's slow and fast axis directions, and the x'-axis and y'-axis in dotted lines denote the slow and fast axis directions of FRM. The rotation angle of these two coordinate axes is θ.

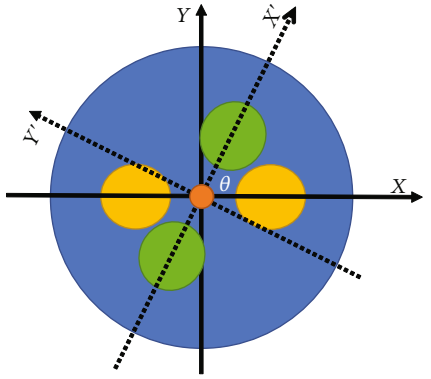

Figure 4: The cross-section of alignment error.

The Jones matrix of FRM is

$$M = M_{\theta\text{out}} M_{\text{Fout}} M_{\text{mir}} M_{\text{Fin}} M_{\theta\text{in}}, \tag{7}$$

where $M_{\theta\text{out}}$ and $M_{\theta\text{in}}$ are the Jones matrix for the fusion point through an angle θ in the backward and forward direction, respectively, M_{Fout} and M_{Fin} represent the Jones matrix for the Faraday rotator through a nonreciprocal angle θ_T backward and forward direction, respectively, and M_{mir} denotes the Jones matrix for the mirror. The details of the matrix are defined in Appendix.

3.2.1. The Faraday Rotator Is Perfect. In this case, $\theta_T = 45$ deg. The Jones matrix for FRM is

$$M = \begin{vmatrix} 0 & 1 \\ -1 & 0 \end{vmatrix}. \tag{8}$$

When the Faraday rotator is perfect, the optical axis

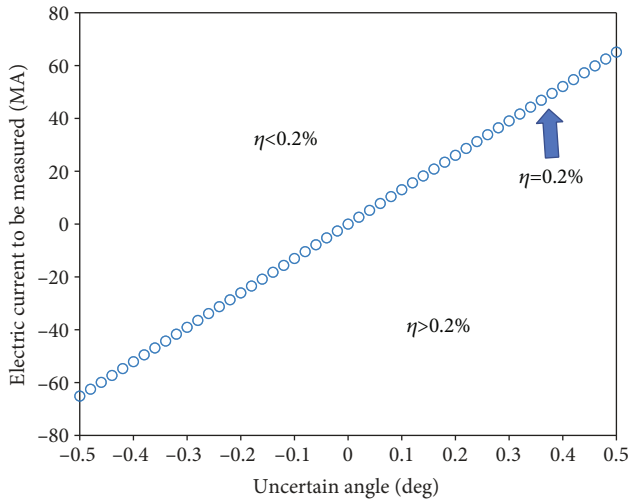

Figure 5: The relationship between the electric current to be measured and the uncertain angle.

misalignment between the sensing fiber and FRM has nothing to do with the system accuracy.

3.2.2. The Faraday Rotator Is Imperfect. In this case, the Jones matrix for FRM is

$$M = \begin{vmatrix} \cos 2\theta_T & \sin 2\theta_T \\ -\sin 2\theta_T & \cos 2\theta_T \end{vmatrix}. \quad (9)$$

When the Faraday rotator is imperfect, the misalignment of the optical axis between the sensing fiber and FRM also has nothing to do with the system accuracy. However, the imperfect Faraday rotator will be the main factor for relative error, which will be discussed in Section 3.3.

3.3. The Effect of the Faraday Rotator. The imperfect Faraday rotator can be divided into two categories. One is the Faraday rotation angle deviated from 45 deg due to the imperfect manufacturing process, and the other is the Faraday rotation angle will change with temperature.

3.3.1. The Effect of the Imperfect Manufacturing Process. When the Faraday rotator is imperfect, the Jones matrix of FRM is represented in Equation (9). The relative error will become

$$\eta = \left| \frac{2\Delta\theta_T}{\theta_F} \right| \times 100\%, \quad (10)$$

where η and θ_F are defined as Equation (3). $\Delta\theta_T = \theta_T - \pi/4$ is the uncertain angle from $\pi/4$ rad. The range of $\Delta\theta_T$ is usually from −0.5 deg to 0.5 deg for commercial products [10]. The number of turns of sensing fiber is 100, and the Verdet constant is 1.1×10^{-6} rad/A. If the relative error equals 0.2%, the relationship between the electric current to be measured and the uncertainty angle is shown in Figure 5.

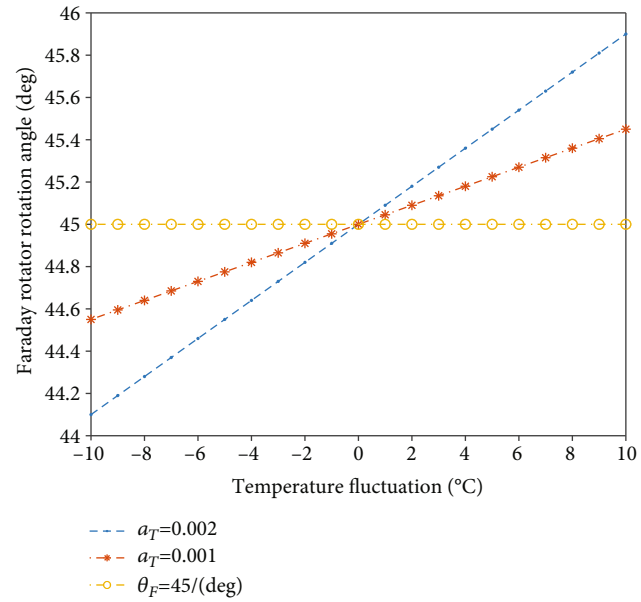

Figure 6: The relationship between the Faraday rotator rotation angle and temperature fluctuation.

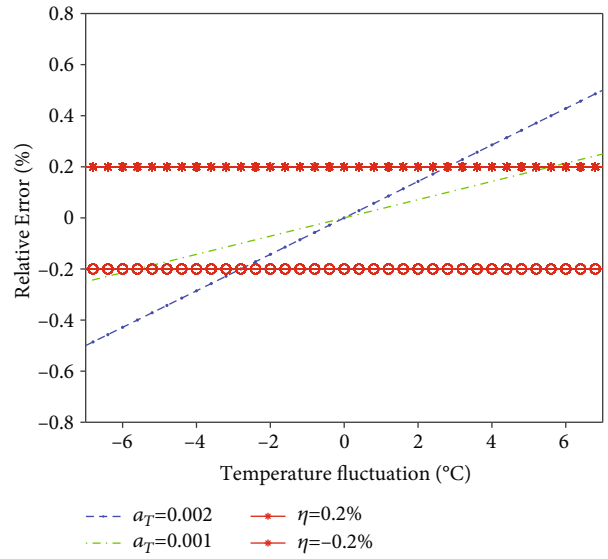

Figure 7: The relationship between relative error and temperature fluctuation.

When the electric current to be measured is on the left and upper of the line, the relative error will meet the measurement requirements. Otherwise, the AFOCS will not meet the system accuracy requirements, as shown in Figure 5.

It should be noted that when the influence of zero bias is eliminated, the error introduced by FRM due to the manufacturing process can be eliminated. The error generated by the Faraday rotator is a fixed additive noise for the SOP rotation angle, so it can be eliminated by subtracting a fixed coefficient.

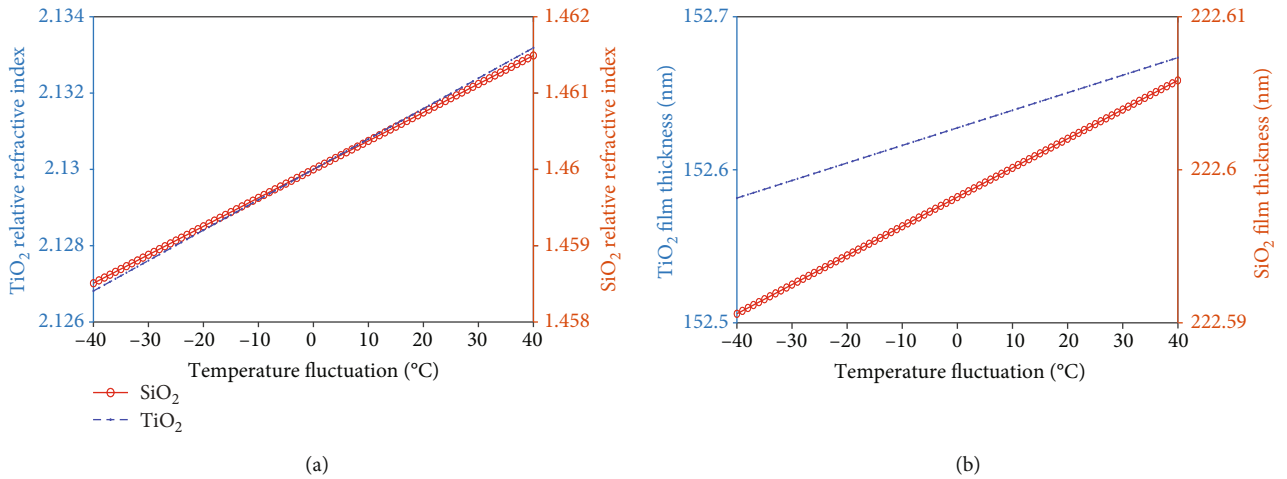

Figure 8: The effect of temperature fluctuation on mirror: (a) the relationship between the relative refractive index and temperature fluctuation and (b) the relationship between the film thickness and temperature fluctuation.

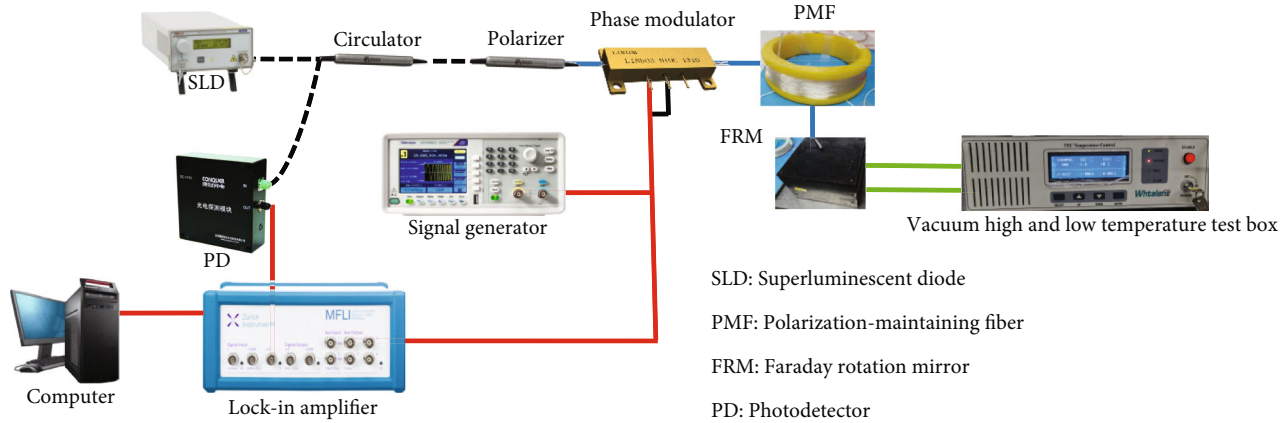

Figure 9: The temperature stability test system of FRM.

3.3.2. The Effect of Temperature. Faraday rotator rotates of the SOP because the ferromagnetic materials provide a constant magnetic field. NdFeB is one kind of ferromagnetic material, which is usually applied to provide a constant magnetic field for a commercial Faraday rotator, but it is sensitive to temperature. When the temperature dependence and the nonlinearity of the magneto-optic material are ignored, the remanence temperature coefficient [28] is given by

$$a_T = \frac{\Delta B_d}{\Delta T \cdot B_d(T_0)}, \tag{11}$$

where $B_d(T_0)$ is the magnetic induction intensity when the temperature is T_0, ΔT represents the temperature fluctuation, T denotes the operation temperature, $\Delta T = T - T_0$, and ΔB_d is the fluctuation of the magnetic induction intensity. The magnetic induction intensity can be given by Equation (12) when the operation temperature is T.

$$B(T) = \Delta B_d + B_d(T_0) = (1 + a_T \Delta T) B_d(T_0), \tag{12}$$

where $B(T)$ is the magnetic induction intensity when the operation temperature is T.

The rotation angle of the Faraday rotator is 45 deg when the temperature is T_0. The Faraday rotation angle is proportional to the magnetic induction intensity, so the Faraday rotator rotation angle can be expressed as Equation (13) when the temperature fluctuation is ΔT.

$$\theta_T = \frac{\pi}{4}(1 + a_T \Delta T), \tag{13}$$

where θ_T is the Faraday rotator rotation angle when the temperature is T. The relationship between the Faraday rotator rotation angle and temperature fluctuation is shown in Figure 6.

The Faraday rotator rotation angle is proportional to the temperature fluctuation, as shown in Figure 6, and the slope is the remanence temperature coefficient. We can get the relationship between the relative error and the temperature fluctuation by Equations (10), (12), and (13). The turns of sensing fiber and the Verdet constant are the same as Section 3.3.2. When the electric current to be measured is 10 kA, the

Table 1: Device model and main parameters.

Name	Brand	Model or main parameters
Light source	Thorlabs China Co., Ltd.	S5FC1018P
Polarizer	MC Fiber Optics Co., Ltd.	The extinction ratio is no less than 28 dB
Circulator	MC Fiber Optics Co., Ltd.	Commercially available
Phase modulator	SWT OPTICS Co., Ltd.	The half-wave voltage is 4 V
Polarization-maintaining fiber	YOFC Optical Fiber and Cable Co., Ltd.	PM1016-A
Faraday rotation mirror	MC Fiber Optics Co., Ltd.	Reflectivity is greater than 99%@1310 nm
Photodetector	Conquer Co., Ltd.	KG-HSP
Lock-in amplifier	Zurich Instruments	MFLI 500 kHz
Signal generator	Tektronix	AFG1062
Vacuum high- and low-temperature test box	Wuhan Tailunte Century Technology Co., Ltd.	TLVB-VHLB50, range: -60°C-100°C, accuracy ± 0.1°C
DC-regulated power supply	Rohde & Schwarz, Munich, Germany	R&S®HMP4000

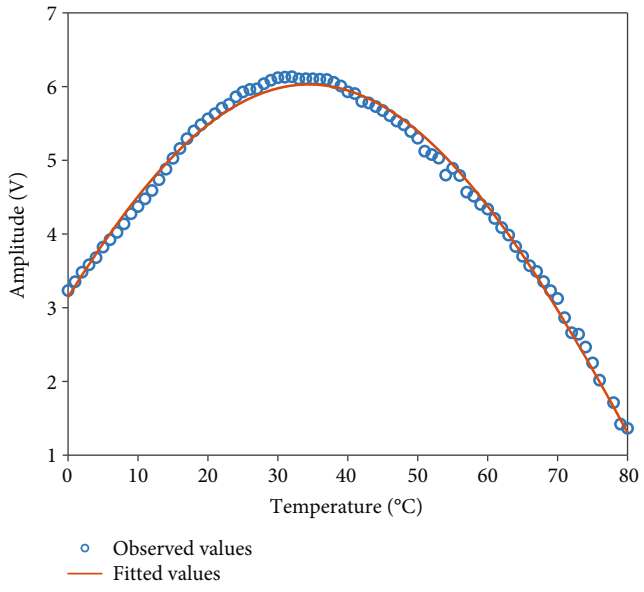

Figure 10: The relationship between correlation demodulation results and temperature.

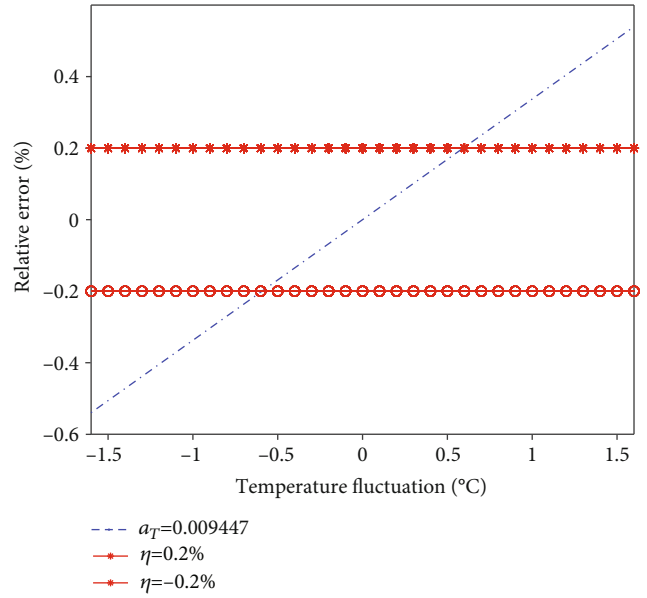

Figure 11: The relationship between relative error and temperature fluctuation.

relationship between relative error and temperature fluctuation is shown in Figure 7.

The range of the operation is within 0.2%; the temperature fluctuation range increases with the remanence temperature coefficient decline, as shown in Figure 7.

3.4. The Effect of the Mirror. To improve the reflectivity and the bandwidth of FRM, the dielectric film mirror composed of alternating films with high and low refractive index is usually applied as the mirror. The influence of temperature on the dielectric film is mainly in two aspects: the thickness and the refractive index. According to Reference [29], as the temperature changes from T_0 to T, the thickness and refractive index of the film are given by Equations (14) and (15).

$$d_{fT} = d_{f0}\left[1 + \left(\alpha_f - B_f\right)\Delta T\right], \tag{14}$$

$$n_f^T = n_{f0} + \left[\left(\frac{dn}{dT}\right)_f \Delta T + \left(1 - n_{f0} - \left(\frac{dn}{dT}\right)_f \Delta T\right)\left(\frac{A_f \Delta T}{1 + (3\alpha_f + A_f)\Delta T}\right)\right], \tag{15}$$

where f is variable and $f = l$ and $f = h$ denote the low- and high-index material, respectively, $A_f = 2(1 - 2\nu_f)(\alpha_s - \alpha_f)/(1 - \nu_f)$, and $B_f = 2\nu_f(\alpha_s - \alpha_f)/(1 - \nu_f)$. α_f and α_s are the thermal expansion coefficients of the film and the substrate, respectively, ν_f denotes the Poisson ratio of film, and $\Delta T = T - T_0$ represents the temperature fluctuation. $(dn/dT)_f$ is the thermal coefficient of the refractive index of the film material. d_{f0} and n_{f0} denote the physical thickness and refractive index of the film, respectively. TiO_2 and SiO_2 are chosen as the high- and low-index material, respectively. Their thermal coefficients of the refractive index of the film

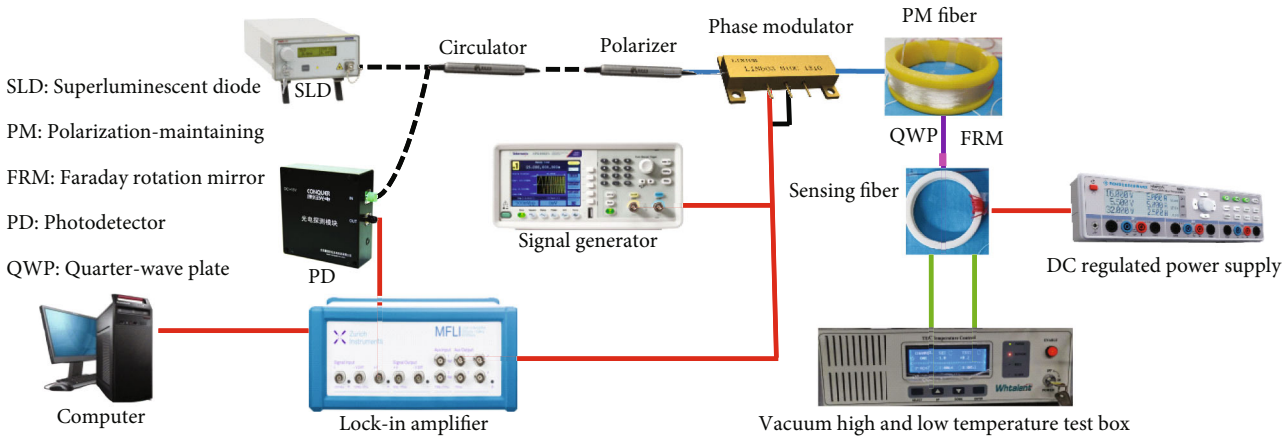

Figure 12: The temperature stability test system of AFOCS.

material are 65×10^{-6}/K and 40×10^{-6}/K, respectively, and the thermal expansion coefficients of them are 7.5×10^{-6}/K and 0.55×10^{-6}/K [29], respectively. The refractive index and the thickness change with temperature fluctuation are shown in Figure 8.

The reflection spectrum of the mirror changes with the thickness and refractive index of the thin film. However, the evolution of the reflection spectrum does not affect the accuracy of the system with the harmonic division demodulation, as described in Section 3.1. Therefore, the influence of temperature on the mirror can be ignored.

4. Experiments and Discussion

4.1. The Effect of Temperature on FRM. The Faraday rotator rotation angle changes with temperature and adversely impacts the system accuracy. The experimental system is designed in Figure 9.

The dotted line denotes the single-mode optical fiber to transmit energy. The polarization-maintaining fiber is represented by the solid blue line to maintain the state of polarization. The solid red line expresses the electronic signal. The temperature control pipeline of the vacuum high- and low-temperature test box is expressed with a double solid line, as shown in Figure 9. The model and main parameters of experimental devices are shown in Table 1.

The temperature of the vacuum high- and low-temperature test box was set from 0°C to 80°C, and the temperature step interval was 1°C. When the temperature reached the set temperature, keep the temperature for 3 minutes before data acquisition to ensure that the FRM had been evenly heated. The data acquisition time is 1 minute, and the mean value is used as the measurement result to eliminate the influence of random noise. The relationship between correlation demodulation results and temperature obtained by the lock-in amplifier is shown in Figure 10.

The hollow dots and the solid lines are the observed and fitted values, as shown in Figure 9. The correlation coefficient is 0.9939, which shows that the fitted values are in good agreement with the experimental values. At this time, the data fitting equation is given by

$$R(T) = a\cos(bT + c) = 6.029\cos(0.02968T - 1.0222). \tag{16}$$

The remanence temperature coefficient is $a_T = 0.009447$ based on Equations (6), (9), (13), and (16). The relationship between the relative error and the temperature fluctuation is shown in Figure 11.

When the relative error is within ±0.2% for power system measurement, the temperature fluctuation range is ±0.6°C, far less than the required working range of AFOCS. Therefore, optimizing the Faraday rotator, such as by vacuum thermal insulation packaging, is necessary to maintain the Faraday rotator in a constant temperature range.

4.2. The Effect of Temperature on AFOCS. We tested the effect of temperature on AFOCS in this section. We introduced a quarter-wave plate and the sensing fiber on the basis of Figure 9, as shown in Figure 12.

The quarter-wave plate was made by ourselves, which is shown with the pink line in Figure 12. The sensing fiber is the spun highly birefringent fiber made from YOFC Optical Fiber and Cable Co., Ltd. The beat length and spin pitch are 10 mm and 5 mm, respectively, as shown in Figure 12.

The temperature of the vacuum high- and low-temperature test box was set from 5°C to 65°C, and the temperature step interval was 2°C. When the temperature reached the set temperature, keep the temperature for 3 minutes before data acquisition to ensure that the sensing head had been evenly heated. The data acquisition time is 1 minute, and the mean value is used as the measurement result to eliminate the influence of random noise. The relationship between the zero drift (the electric current was set to zero) of the system and temperature is shown in Figure 13.

The hollow dots and the solid lines are the observed and fitted values, as shown in Figure 9. The correlation coefficient is 0.9867, which shows that the fitted values are in good

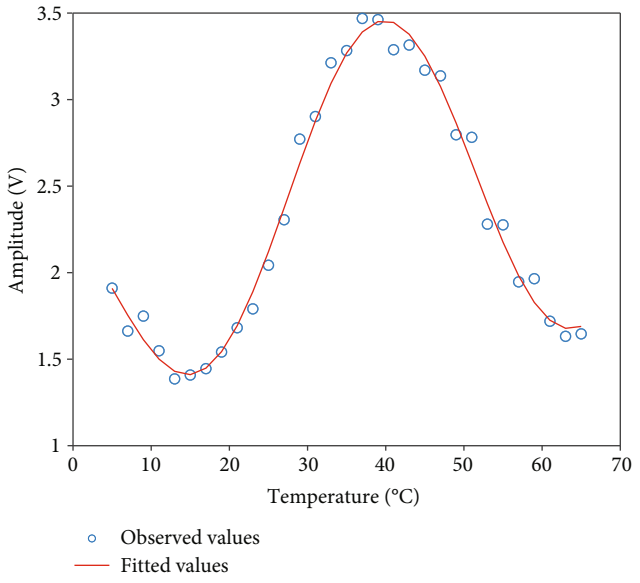

FIGURE 13: The relationship between the temperature and output of AFOCT.

agreement with the observed values. At this time, the data fitting equation is given by

$$R'(T) = a_1 \sin(b_1 T + c_1) + a_2 \sin(b_2 T + c_2) = A(T) + B(T), \tag{17}$$

where $a_1 = 2.71$, $b_1 = 0.02347$, $c_1 = 0.5561$, $a_2 = 0.7596$, $b_2 = 0.1414$, and $c_2 = 2.261$. The remanence temperature coefficient is 0.007113. The fitted function could be regarded as the sum of two functions. One is related to the Verdet constant and the quarter-wave plate ($B(t)$), and the other is related to the FRM ($A(t)$). The remanence temperature coefficient is a little different from a_T obtained in Section 4.1. The reason may be some errors generated during the fusion process of the sensing optical fiber.

5. Conclusion

As an essential part of AFOCS, the influence of FRM is analyzed in this paper. The conclusion can be summarized as follows.

Firstly, harmonic division demodulation is better than the first harmonic method to copy with the fluctuation of light intensity, which is caused by long-term operation or the effect of the temperature fluctuation on the thin film mirror.

Secondly, the optical axis misalignment between the sensing fiber and FRM has nothing to do with the relative error. So the single-mode fusion splicer can be applied in this fusion splicing process.

Thirdly, the influence of temperature on the Faraday rotator determines the performance of the reflection unit. The temperature fluctuation range is related to the measured electric current to satisfy the required accuracy for IEC 60044-8 class 0.2S if the FRM does not work at a stable temperature.

Appendix

The direction from the light source to the Faraday rotation mirror (FRM) is defined as the forward direction, and the direction from FRM to the photodetector is defined as the backward direction. $M_{\theta\text{out}}$ and $M_{\theta\text{in}}$ are the Jones matrix for the fusion point through an angle θ in the backward and forward direction, respectively. The Jones matrix for the fusion point is given by

$$M_{\theta\text{out}} = \begin{vmatrix} \cos\theta & -\sin\theta \\ \sin\theta & \cos\theta \end{vmatrix}, \tag{A1}$$

$$M_{\theta\text{in}} = \begin{vmatrix} \cos\theta & \sin\theta \\ -\sin\theta & \cos\theta \end{vmatrix}, \tag{A2}$$

where M_{Fout} and M_{Fin} represent the Jones matrix for the Faraday rotator through an angle θ_T backward and forward direction, respectively. The Jones matrix for the Faraday rotator is given by

$$M_{\text{Fout}} = \begin{vmatrix} \cos\theta_T & -\sin\theta_T \\ \sin\theta_T & \cos\theta_T \end{vmatrix}, \tag{A3}$$

$$M_{\text{Fin}} = \begin{vmatrix} \cos\theta_T & -\sin\theta_T \\ \sin\theta_T & \cos\theta_T \end{vmatrix}. \tag{A4}$$

The Jones matrix for the mirror is given by

$$M_{mir} = \begin{vmatrix} 1 & 0 \\ 0 & 1 \end{vmatrix}. \tag{A5}$$

Data Availability

Data underlying the results presented in this paper are not publicly available at this time but may be available from the corresponding author upon request.

Conflicts of Interest

The authors declare no conflict of interest.

Acknowledgments

The authors would like to thank anyone who puts forward constructive suggestions.

References

[1] S. Dass and R. Jha, "Micrometer wire assisted inline Mach-Zehnder interferometric curvature sensor," *IEEE Photonics Technology Letters*, vol. 28, no. 1, pp. 31–34, 2016.

[2] M. Y. Li, R. Singh, C. Marques, B. Zhang, and S. Kumar, "2D material assisted SMF-MCF-MMF-SMF based LSPR sensor for creatinine detection," *Optics Express, Article*, vol. 29, no. 23, pp. 38150–38167, 2021.

[3] Y. Wang, G. Zhu, M. Y. Li et al., "Water pollutants p-cresol detection based on au-ZnO nanoparticles modified tapered optical fiber," *IEEE Transactions on Nanobioscience*, vol. 20, no. 3, pp. 377–384, 2021.

[4] M. Y. Li, R. Singh, M. S. Soares, C. Marques, B. Zhang, and S. Kumar, "Convex fiber-tapered seven core fiber-convex fiber (CTC) structure-based biosensor for creatinine detection in aquaculture," *Optics Express*, vol. 30, no. 8, pp. 13898–13914, 2022.

[5] G. Zhu, Y. Wang, Z. Wang et al., "Localized plasmon-based multicore fiber biosensor for acetylcholine detection," *IEEE Transactions on Instrumentation and Measurement*, vol. 71, pp. 1–9, 2022.

[6] R. Wang, S. Xu, W. Li, and X. Wang, "Optical fiber current sensor research: review and outlook," *Optical and Quantum Electronics*, vol. 48, no. 9, pp. 1–22, 2016.

[7] S. Kucuksari and G. G. Karady, "Experimental comparison of conventional and optical current transformers," *IEEE Transactions on Power Delivery*, vol. 25, no. 4, pp. 2455–2463, 2010.

[8] X. Wang, F. Ma, J. Yu, X. Liu, and N. Song, "Design of the portable fiber-optic current transformer for electrolytic aluminum industry," *Optik*, vol. 205, p. 164187, 2020.

[9] J. Zhao, L. Shi, and X. H. Sun, "Design and performance study of a temperature compensated ±1100kV UHVDC all fiber current transformer," *EEE Transactions on Instrumentation and Measurement*, vol. 70, no. 6, p. 7001206, 2021.

[10] D. Karabulut, A. Miazin, A. Gusarov et al., "Effect of Faraday mirror imperfections in a fiber optic current sensor dedicated to ITER," *Fusion Engineering and Design*, vol. 138, pp. 48–52, 2019.

[11] J. Wu, X. Zhang, L. Chen, and B. Wu, "Research on measurement technology of ship leakage current by all-fiber optic current sensor," *IEEE Access*, vol. 9, pp. 160268–160276, 2021.

[12] R. C. Li, J. Zhao, and D. C. Li, "Impact of polarizer on reflecting fiber-optic current transducer," *Journal of Applied Optics*, vol. 33, no. 1, pp. 216–219, 2012.

[13] J. Yu, C. X. Zhang, C. S. Li, X. X. Wang, Y. Li, and X. J. Feng, "Influence of polarization-dependent crosstalk on scale factor in the in-line Sagnac interferometer current sensor," *Optical Engineering*, vol. 52, no. 11, p. 117101, 2013.

[14] F. Ferdous, A. H. Rose, and P. Perkins, "Passively biased inline Sagnac interferometer-optical current sensor: theoretical review," *Optical Engineering*, vol. 60, no. 5, p. 057102, 2021.

[15] X. X. Wang, Z. J. Zhao, C. S. Li, J. Yu, and Z. J. Wang, "Analysis and elimination of bias error in a fiber-optic current sensor," *Applied Optics*, vol. 56, no. 32, pp. 8887–8895, 2017.

[16] J. Wu, X. Zhang, L. Chen, and B. Wu, "Simulation analysis of temperature effects on all-fiber optic current sensor," *Energy Reports*, vol. 7, pp. 1521–1528, 2021.

[17] X. M. He, G. C. Wang, W. Gao, Y. G. Wang, and H. Z. Gao, "The effect analysis of impact on a fiber optic current sensor," *Optik*, vol. 238, p. 166724, 2021.

[18] L. Wang, "Modeling and simulation of polarization errors in reflective fiber optic current sensor," *Optical Engineering*, vol. 50, no. 7, p. 074402, 2011.

[19] X. C. Wang, W. N. Zhou, and Y. Qin, "SNR of optical fiber current sensor reaching 02 accuracy class," *Infrared and Laser Engineering*, vol. 43, no. 11, pp. 3704–3708, 2014.

[20] P. Drexler and P. Fiala, "An optical boiler generating singlet oxygen O2(a1Δg)," *Radio Engineering*, vol. 38, no. 12, pp. 1179–1182, 2008.

[21] L. Sun, S. B. Jiang, and J. R. Marciante, "All-fiber optical Faraday mirror using 56-wt%-terbium-doped fiber," *IEEE Photonics Technology Letters, Article*, vol. 22, no. 13, pp. 999–1001, 2010.

[22] Y. K. Wang, Z. P. Wang, and S. Sun, "Effects of temperature characteristic of Faraday rotator on passively demodulated all-optical fiber current transformers," *Power System Technology*, vol. 37, no. 1, pp. 206–210, 2013.

[23] J. Li-yuan, L. Ding-quan, M. Chong, C. Qing-yuan, and G. Ling-shan, "Influence of temperature variation on polarization characteristics of silver thin film mirror," *Chinese Optics*, vol. 11, no. 4, pp. 604–609, 2018.

[24] J. Blake, P. Tantaswadi, and R. Carvalho, "In-line Sagnac interferometer current sensor," *IEEE Transactions on Power Delivery*, vol. 11, no. 1, pp. 116–121, 1996.

[25] W. Cai, J. H. Xing, and Z. Y. Yang, "Contributions to Verdet constant of magneto-optical materials," *Acta Physica Sinica*, vol. 66, no. 18, p. 187801, 2017.

[26] *International Standard for Current Transformers*, International Electrotechnical Commission (IEC), Geneva, Switzerland, 1987.

[27] F.-b. Pang, Y. Liu, Y.-b. Yuan, and L. Gao, "Influencing factors analysis on the detector output signal of fiber optic current transformer with sine modulation," *Measurement*, vol. 151, p. 107151, 2020.

[28] Y. X. Chen, "Digital display and automatic recording of magnetic temperature coefficient test," *Application of Electronic Technique*, vol. 2, pp. 32–34, 1980.

[29] S. H. Kim and C. K. Hwangbo, "Derivation of the center-wavelength shift of narrow-bandpass filters under temperature change," *Optics Express*, vol. 12, no. 23, p. 5634, 2004.